ADVANCED MATERIALS

Polymer Optical Fibers and Nonlinear Optical Device Principles**

Optoelectronics
Active LB Layers
Model Calculations
Fluorinated Polymers
Network Systems

By W. Groh, D. Lupo and H. Sixl*

Dedicated to Professor Wolfgang Hilger on the occasion of his 60th birthday

Basic principles of the present optoelectronic research activities at Hoechst AG are presented in this contribution. Within the diversified broad band spectrum of optoelectronic materials and applications our interest is focused on new types of polymer optical fibers and nonlinear optical device principles using organic Langmuir–Blodgett films and electrically poled polymers. The basic principles and the limits of the present research and development activities which have a high market potential are outlined.

1. Introduction

Polymeric materials have developed extraordinarily quickly in the last fifty years and now rank among the most important materials used in society and in industrial applications. New polymers with unusual optical and electrical properties are predicted to have a high market potential in the future. The combination of electrical and optical properties is especially attractive in modern electronics which develops more and more in the direction of optoelectronics with long term ambitions concerning all-optical devices. Optoelectronics plays a central role in computing and the handling of large amounts of data. Consequently material research using functionalized polymers with specially designed tailor-made properties becomes very important.

In the last few years, interest in polymer optical fibers (POF) has increased because of their low cost, easy handling and good flexibility even at large diameters.[1–5] These fibers are used for short-haul data transmission applications in computer links or in automobiles. However, the presently available fibers suffer from two major disadvantages, namely the relatively high loss of about 200 dB/km and the low maximum operating temperature of 80 to 90 °C, which is not sufficient for automotive applications. In distributed networks, even for short distance transmission, improvements in the optical loss are essential as will be shown in this contribution.

Nonlinear optical (NLO) effects have long ceased to be only a research curiosity or even research tool, and are being widely investigated and used in integrated optics and optoelectronic applications. For example, the electro-optic effect is used to build commercially available ultrafast electro-optic modulators, based on lithium niobate, which can modulate a continuous wave (CW) laser at multi-GHz frequencies. There are indications that for certain applications, organic materials will show significantly better performance than inorganic ones. The reasons for interest in organic materials and some of the problems to be solved before they can be used commercially are discussed in Section 3.

2. Polymer Optical Fibers

2.1. Model Calculations

The two important intrinsic loss factors in commercial polymethylmethacrylate (PMMA) optical fibers are C–H overtone absorption and Rayleigh scattering, which is mainly due to microscopic density fluctuations. Both factors lead to a theoretical lower loss limit of about 100 dB/km at 650 nm[1] with 90 dB/km due to overtone absorption as seen from Figure 1. Reduction of the loss is achieved by substituting the hydrogen atoms with heavier elements like deuterium which have lower energy absorption bands.

Deuteration, however, is a very expensive process and therefore other substituents have to be considered. Fluorination, for example, seems to be a good choice, but there is no information available in the literature about the positions and intensities of higher C–F vibrational overtones.

Light transmission measurements on perfluorinated compounds for a sample thickness of 10 cm show no C–F absorption in the visible spectral region as shown in Figure 2. Although this gives an upper limit for the C–F loss contribution the measurement is not sensitive enough to predict what loss a fiber consisting of this material would have, because

[*] Prof. H. Sixl, Dr. W. Groh, Dr. D. Lupo
Angewandte Physik, Hoechst AG
P.O. Box 800320, D-6230 Frankfurt am Main 80 (FRG)

[**] This work was supported by the Federal Ministry of Research and Technology (BMFT). The research projects are done in cooperation with other industrial and academic partners. We would like to thank our colleagues active in the project teams for many stimulating discussions and efficient cooperation.

ADVANCED MATERIALS

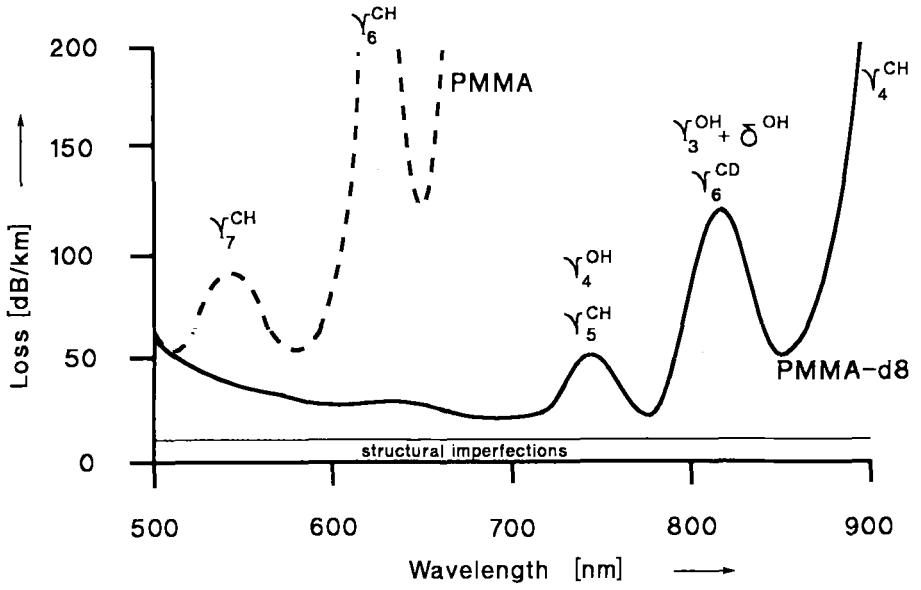

Fig. 1. Spectral loss of polymethylmethacrylate (PMMA) and d_8-PMMA polymer optical fibers.

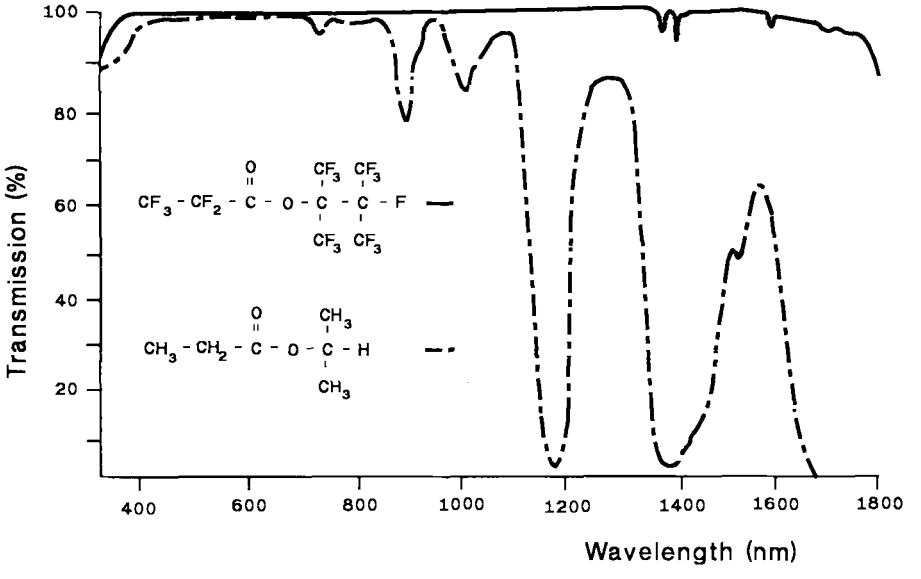

Fig. 2. Transmission spectra of a partially fluorinated and a perfluorinated compound (sample length: 10 cm).

the length of the fiber is 10^4 to 10^5 times larger. Therefore theoretical calculations on the expected overtone band positions and intensities have been made.[4-6]

Overtone bands appear because molecular vibrations are not perfectly harmonic. This is expressed in a nonsymmetric potential curve and a non-zero anharmonicity constant x. From the Morse potential approximation (Fig. 3) we obtain the energy levels and the corresponding transitions. We can calculate the spectral position of any overtone band if we know the position of the fundamental vibration and the anharmonicity constant. From infrared spectroscopic data on hydrogenated, deuterated or halogenated compounds one can find ν_1 and also ν_2 for all interesting vibrations, from which the x-values can be calculated. If, for example, ν_1 and ν_2 were known for a certain molecular vibration, the positions of all higher overtones can be calculated.

Energy levels (Morse potential)

$$G(v) = \nu_0(v + \tfrac{1}{2}) - \nu_0 x(v + \tfrac{1}{2})^2$$

Transitions

$$\nu_v = G(v) - G(0) \rightarrow \boxed{\nu_v = \frac{\nu_1 v - \nu_1 x v(v+1)}{1 - 2x} \qquad v = 2,3,4,\ldots}$$

or if e.g. ν_1 and ν_2 are known $\Rightarrow x$

For experimentally accessible overtones, for example from C–H or C–D vibrations, one can evaluate the band strength from the spectrum if the number of contributing bonds,

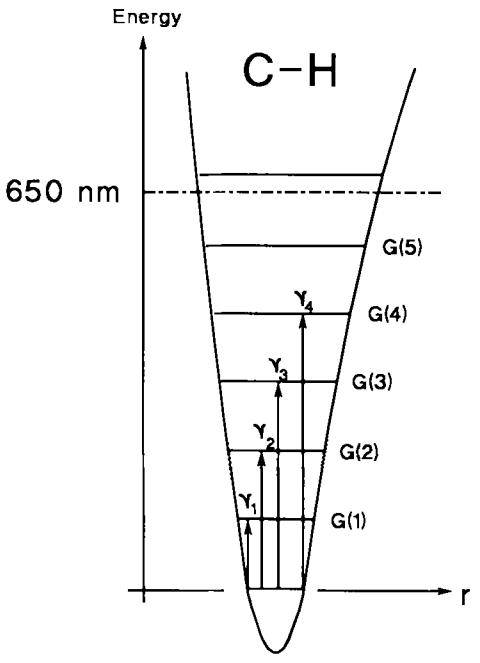

Fig. 3. Calculation of molecular vibrations with the Morse potential approximation.

molecular weight, density and sample thickness are known. Theoretical calculation of the interesting vibrations is also possible (with some approximations) due to the work of *Timm* and *Mecke*.[6, 7] We come out with a very simple equation for the band strength of an overtone normalized to the band strength of its fundamental. Any overtone band strength can be calculated if we know the anharmonicity constant x and the fundamental band strength $E(\nu_1)$, both of which can be extracted from an infrared spectrum of an appropriate compound.

This is illustrated in Figure 4, which shows selected parts of the infrared spectrum of a fluorinated model compound. Shown are the fundamental and overtone vibrational bands of the carbonyl group. From such spectra the exact band positions and intensities can be easily extracted. If, for example, the spectral positions of ν_1 and ν_2 are known, the anharmonicity constant and the positions of all other overtones can be calculated as shown above. We also obtain the band strength of the fundamental and can thus calculate all band strengths of the higher overtones which are not experimentally accessible.

The most important molecular vibrations in polymers are listed in Table 1. In a fluorine-containing methacrylate com-

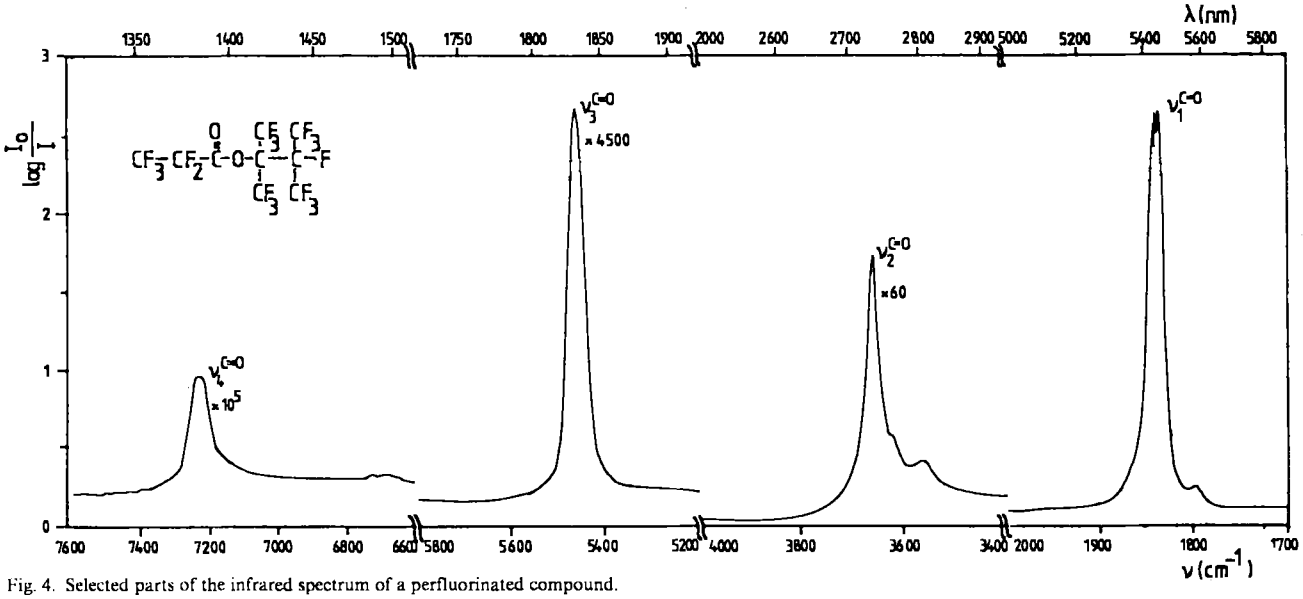

Fig. 4. Selected parts of the infrared spectrum of a perfluorinated compound.

Hans Sixl studied physics at the University of Stuttgart, FRG, gaining a Ph.D. in 1971 and habilitating in 1976. After this he spent some time at the Max Planck Institute for Solid State Research in Stuttgart and also in Grenoble working with Professor Dransfeld before returning to Stuttgart University to become Professor of Physics in 1981. Since 1986 he has been the Departmental Head of Applied Physics at Hoechst in Frankfurt, FRG.

ADVANCED MATERIALS

pound we have to consider the absorption due to the C–H bonds, the carbonyl group and the C–F bonds. Values for the spectral position of the fundamental, the band strengths and the anharmonicity constants are also given in Table 1. The C–H absorption is most pronounced because of its large anharmonicity constant.

Table 1. Important molecular vibrations in organic polymers.

bond	ν_1 [cm^{-1}]	$E(\nu_1)$ [cm mol^{-1}]	x	overtone quantum number in VIS
C–H	2950	6×10^5	1.9×10^{-2}	~ 5
C–D	2230	2.4×10^5	1.46×10^{-2}	~ 8
C=O	1846	9.6×10^6	6.5×10^{-3}	~ 9
C–F	1250	2.4×10^7	4×10^{-3}	~13
C–Cl	770	4.8×10^6	5.9×10^{-3}	~23

C–C and C–O vibrations cannot be treated using this simple model, because the dipole curves are much more complex and the approximation of a smooth dipole curve no longer holds. The spectral positions of the fundamental vibrations are known from the literature but there is little or no information about the corresponding overtone wavelengths and intensities. The intensity of the absorption of the C–C group, for example, depends strongly on the symmetry of the C–C bonds. There is experimental evidence that the fourth overtones of the C–C and C–O groups, expected in the 1200–1500 nm range, are already undetectable.[8, 9]

The results of the calculations are summarized in Figure 5. The symbols represent the calculated spectral overtone positions and the corresponding calculated band strengths. For the experimentally accessible low order C–H, C–D and C=O overtones we found very good agreement for the band positions. Experimental and theoretical band strengths coincide within a factor of 3 which is very good for such a simple model and sufficient for these considerations. The results for the experimentally inaccessibly high C–F and C=O, and also for C–Cl overtones are given. In the most important spectral region between 600 and 900 nm they are orders of magnitude lower in intensity than the C–H overtones and therefore should contribute negligibly to the losses in the fiber. The reasons are, firstly, the low anharmonicity constant of the C–F, C–Cl and C=O vibrations compared to C–H and, secondly, the low energy fundamentals which are in the far infrared. To get absorption in the visible spectral region, relatively high quantum states have to be excited which are therefore low in band strength. These are the two important factors dominating the absorption in the visible region.

The theoretical lower loss limit for fully halogenated polymers in the 600–900 nm region is therefore limited by Rayleigh scattering which is about 10 dB/km at 650 nm. From the theoretical point of view losses of a few dB/km should be attainable with optimized perfluorinated polymers.

Other expected advantages of fluorination are

- less scattering
- improved transparency at longer wavelengths where fast high power LEDs are available
- lower water uptake
- usually higher glass transition temperature.

The lower scattering losses of fluorinated polymers can be easily understood by considering the parameters responsible for scattering (Table 2). In the case of density fluctuations the loss is proportional to the eighth power of the refractive

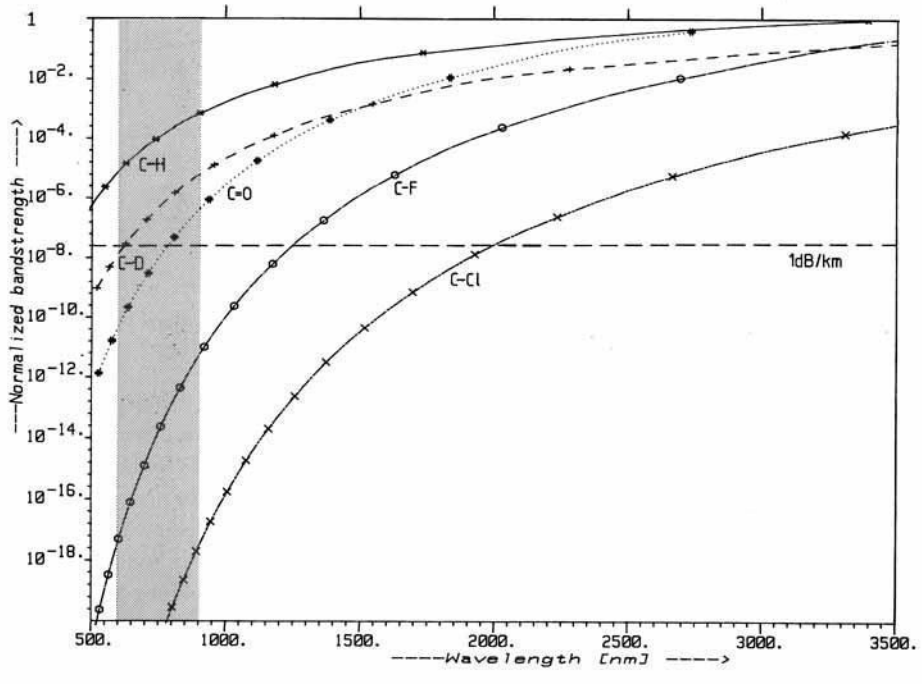

Fig. 5. Calculated spectral overtone positions and normalized integral band strengths for different C–X vibrations. The marked zone denotes the important spectral region for polymer optical fibers.

Density fluctuations

$$D_D \sim \frac{1}{\lambda^4} n^8 \beta_T$$

Anisotropy fluctuations

$$D_A \sim \frac{I}{\lambda^4} n^4 N p \delta_0^2$$

Concentration fluctuations

where λ: wavelength. n: refractive index. β_T: isothermal compressibility. N: monomer concentration in the polymer. p: number of parallel monomers per structural unit. δ_0: monomer anisotropy.

index. It is known that fluorination reduces the refractive index and thus leads to less scattering. The same is true for anisotropy fluctuations which are pronounced in polymers with aromatic groups. In special cases like copolymers or polymer blends, additional inhomogeneities on the molecular scale have to be considered. They are very difficult to predict theoretically because of unknown interaction parameters and exact microscopic structures.

Unfortunately a complete fluorination seems to be impossible from a chemical point of view. Our investigations showed that completely halogenated monomers do not polymerize well. Two or three C–H or C–D groups have to remain in the molecule and therefore a realistic lower loss limit for existing fluoropolymers is in the 40–70 dB/km range.

2.2. Local Area Networks

In POF-Network-Systems the fiber loss is an important factor but the total flux budget also depends on the system configuration and the properties of the active and passive components.

In Figure 6a and b two basic network topographies, the tapped bus and the star bus are compared. Calculating the total path attenuation we consider the fiber attenuation, average connector losses of 1 dB, typical POF-coupler losses and also different LED-output powers for different data rates.

To simplify the calculations a circular arrangement of nodes has been assumed. In the tapped bus network the coupler losses are divided into the insertion loss, the tap loss and the coupling loss. Typical values for commercial taps are given in Table 2. The worst case of path loss can be calculated using the equation under Table 2, where α_c is the connector loss, α_f the fiber loss, and N the number of nodes.

In a passive star bus network the nodes are connected by polymer optical fibers via a star coupler (Fig. 6b). In this system we have a splitting loss due to the equal intensity

Table 2. Optical properties of the tapped bus network topography.

	Loss values of the tap	
loss	definition	value [dB]
Tap	$-10 \log (P_3/P_1)$	9
Insertion	$-10 \log (P_2/P_1)$	1
Coupling	$-10 \log (P_2/P_4)$	4

$\alpha_{TB} = \alpha_{coup} + 2N\alpha_c + (N-2)\alpha_{in} + \alpha_{tap} + \alpha_f 2\pi R$

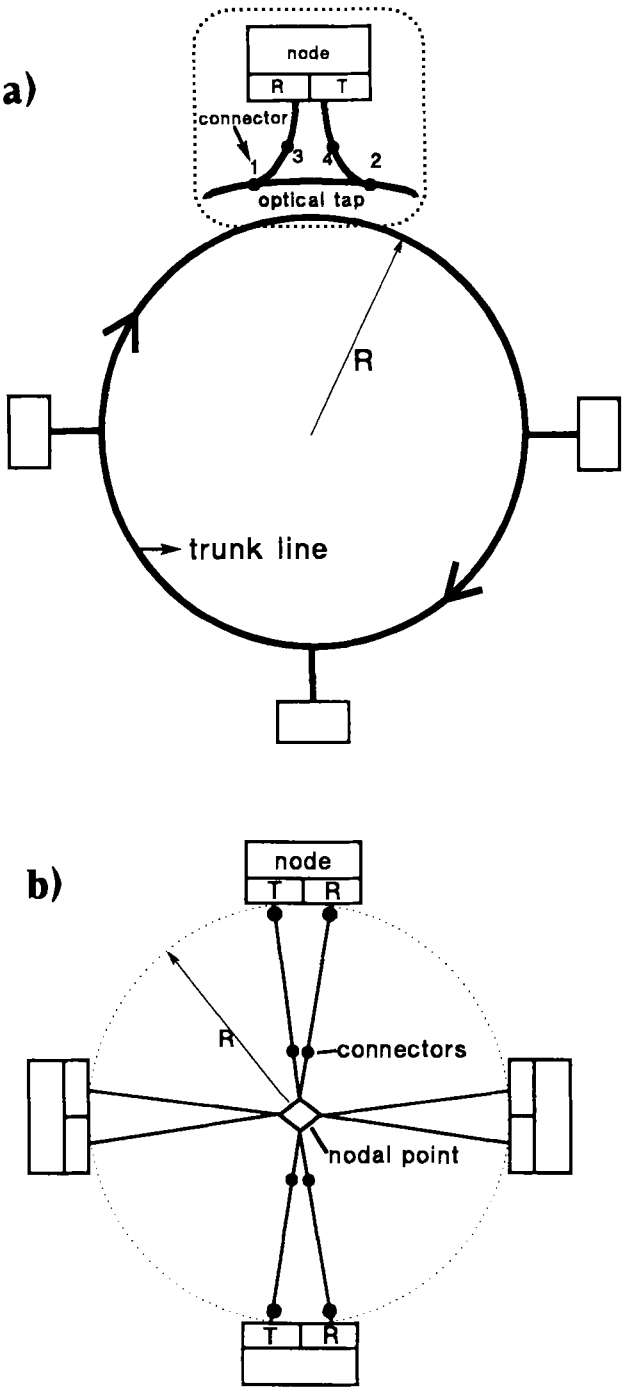

Fig. 6. Basic network topographies. a) Tapped bus network. b) Star bus network.

splitting to all nodes and an excess loss in the mixing region. The worst case of path attenuation can be calculated using the equation under Table 3. The system has four connectors, the excess loss depending on the number of nodes, the splitting loss which is 10 log N, and 2 R is the distance between an LED and a receiver. In a tapped bus the flux budget decreases linearly with the number of nodes, while for the star bus it decreases in proportion to the logarithm of the number of nodes.

ADVANCED MATERIALS

Table 3. Optical properties of the star bus network topography.

Loss values of the star		
nodes N	excess loss α_e [dB]	splitting loss α_{split} [dB]
2	1.5	3
4	2.5	6
6	3	7.8
8	3	9
10	3.5*	10

* extrapolated value

$\alpha_{SB} = 4\alpha_c + \alpha_c(N) + 10 \log N + \alpha_f \times 2R$

while for the star bus it decreases in proportion to the logarithm of the number of nodes.

Figure 7a shows the system budget for the tapped and star bus topography as a function of the number of nodes. The full lines correspond to a network radius of 2 meters, the dashed lines to 10 meters and the dashed-dotted lines to 50 meters radius. The horizontal lines at 16 dB and 28 dB indicate the flux ratio available for the network systems with 1.5 Mbaud and 40 Kbaud, respectively. The calculations were done for a PMMA fiber with 210 dB/km loss. Taking into account a system margin of 3 dB, only 3–5 subscribers can be connected via a star coupler in very local area networks like, for example, automobiles or robots. For short-haul, low data transmission, multinoded star-bus networks can be realized. Tapped bus systems only allow for low data transmission rates in networks of about 2 m size.

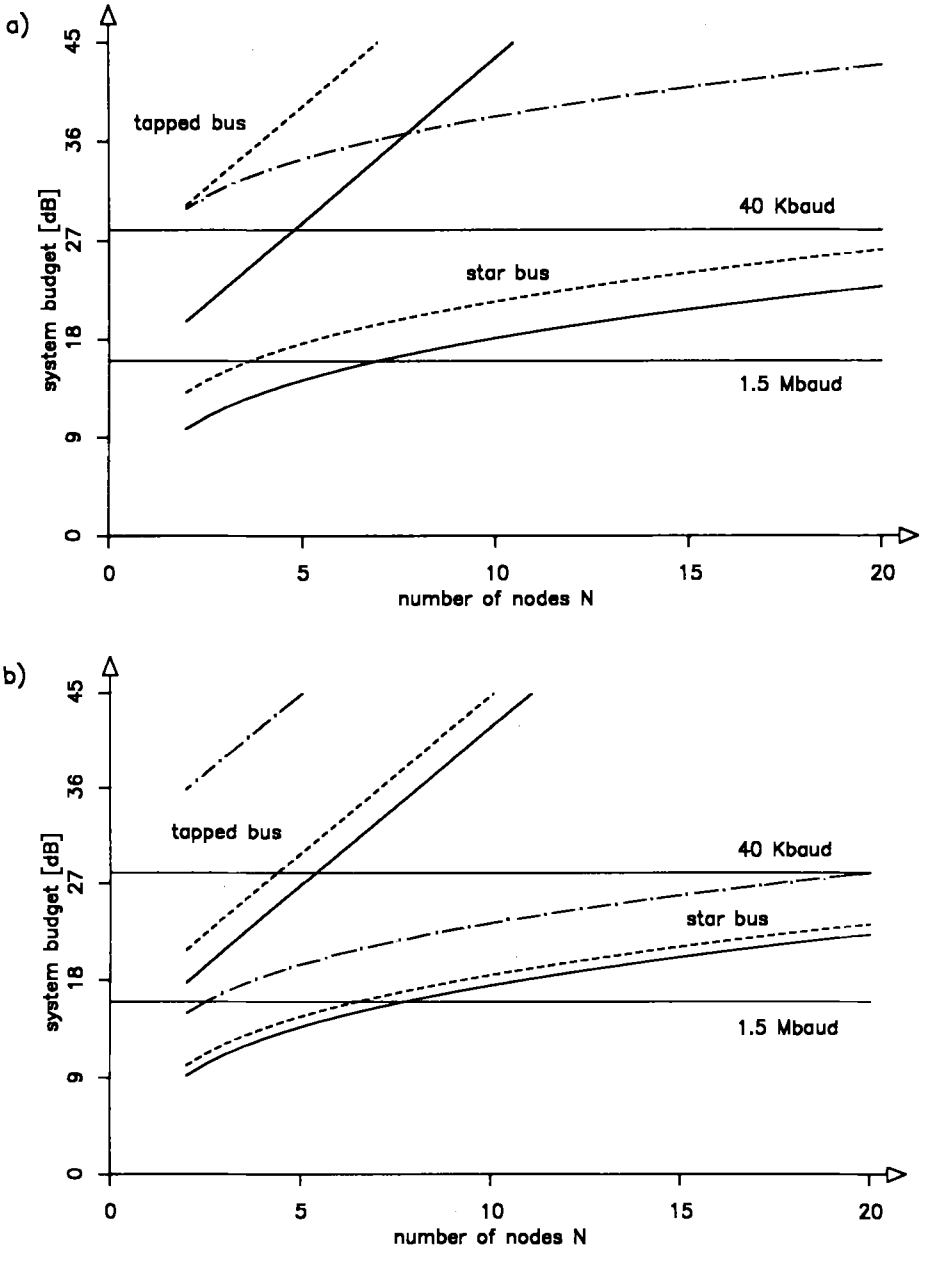

Fig. 7. System budget for tapped and star bus networks. a) Fiber loss: 210 dB/km. b) Fiber loss: 60 dB/km. The different network radii R = 2, 10, 50 meters are represented by full, dashed and dashed-dotted curves, respectively. The horizontal lines mark the assumed flux ratios of 28 and 16 dB for the indicated data transmission rates.

In very local area networks the system loss is mainly determined by the coupler losses and only to a much smaller degree by the fiber attenuation. For a radius of 2 meters, for example, the fiber loss contributes only 1 or 2 dB.

This can also be seen in Figure 7b, for which a fiber loss of only 60 dB/km was assumed. From the loss consideration explained above, 60 dB/km seems to be a realistic value for the loss of an optimized fluorinated polymer in the visible spectral region.

For very short distances the star bus system budgets do not differ significantly, due to the minor influence of the fiber attenuation compared to the coupler losses. For longer distances like 50 or 100 meters the improved fiber loss allows for multinoded star bus networks with a 40 Kbaud data rate, which is not possible with today's PMMA fibers. Even with a low loss fiber, high data rate applications can only be covered if not more than about 5 subscribers are connected. For tapped bus systems only very local area networks (2–10 m) with low data rates and not more than 5 subscribers are possible.

In conclusion a star bus system has the advantage of lower path attenuation, so a larger number of subscribers can be connected; it requires less receiver dynamic range, but the system has a larger overall fiber length. More complex systems can be made with a low loss fiber but the data rates have to be low and the system is still of limited size.

With the performances of the present active and passive components no complex high speed networks, working above 1 Mbaud, can be realized. To achieve a higher flux ratio improvements have to be made not only on passive components like fibers and couplers but also on transmitters and receivers.

3. Organic Materials for Nonlinear Optics

3.1. Basic Principles

The term "nonlinear optics" refers to effects which depend on quadratic or higher powers of the electric field strength. The interaction of an electric field $\vec{E}$ with a material can be described using a power series of the net polarization $\vec{P}$ of the material (Eq. 1).

$$\vec{P} = \vec{P}_0 + \chi^{(1)} \cdot \vec{E} + \chi^{(2)} : \vec{E}\vec{E} + \chi^{(3)} : \vec{E}\vec{E}\vec{E} + \ldots \quad (1)$$

$\chi^{(n)}$ is the nth order susceptibility which is a $(n+1)$th rank tensor. $\chi^{(1)}$ is responsible for the well known "linear" phenomenon of refraction. $\chi^{(2)}$, upon which we shall concentrate here, leads to quadratic effects such as optical second harmonic generation (SHG), parametric frequency mixing and the linear electro-optic effect. $\chi^{(3)}$ leads to such effects as intensity-dependent refractive indices and coherent anti-Stokes Raman spectroscopy (CARS).[10] Since the higher order susceptibilities are normally much smaller than $\chi^{(1)}$ nonlinear effects become noticeable only at high electric field strength, i.e. with lasers or with relatively high voltages over small distances.

In the mid-1970s it was discovered that certain types of organic molecules have much higher second-order nonlinearities and shorter switching times than the known inorganic materials such as potassium dihydrogen phosphate or lithium niobate.[11] The common characteristic of most such

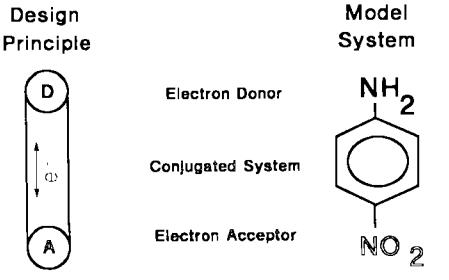

Fig. 8. Molecular design principle for high β species and the model system *p*-nitroaniline.

molecules is the presence of a conjugated π-electron system, providing easily polarized electrons, and donor and acceptor groups which provide the necessary asymmetry for second order effects. The design principles and a model system are shown in Figure 8. In organic systems one can thus speak of a *molecular* basis for the nonlinearity resulting from a polarization $\vec{p}$ of the charges in an individual molecule (Eq. 2).

$$\vec{p} = \vec{\mu}_0 + \alpha \cdot \vec{E} + \beta : \vec{E}\vec{E} + \gamma : \vec{E}\vec{E}\vec{E} + \ldots \quad (2)$$

where β and γ are the 2nd and 3rd order hyperpolarizabilities and μ_0 is the molecular dipole moment, although the absolute determination of these quantities presents considerable problems.[12]

A large value of β is not a sufficient condition for a high second order macroscopic susceptibility $\chi^{(2)}$, which is only non-zero for non-centrosymmetric systems. Furthermore the individual molecules should be aligned so that the individual nonlinearities add to each other as much as possible. β is related to $\chi^{(2)}$ through the relation (Eq. 3).

$$\chi^{(2)} = N \mathrm{F} \mathrm{D} \beta \quad (3)$$

where N is the density of nonlinear species, F stands for local-field correction factors and D stands for the effect of molecular orientation in converting from molecular coordinates and nonlinearity to macroscopic effects. Within the (sometimes questionable[13]) assumption that the molecular nonlinearity is dominated by the component β_{zzz} along the chromophore axis, a perfectly parallel orientation along the z-axis would for example lead to a maximum value of $\chi^{(2)}_{zzz}$. Of course such perfect orientations are practically nonexistent and can only be approximated.

Three main techniques are available to achieve a non-centrosymmetric orientation of the chromophores. One possi-

ADVANCED MATERIALS

bility is design of the molecule so that it crystallizes noncentrosymmetrically. High $\chi^{(2)}$ values and good quality single crystals have been achieved for several compounds,[14-16] and one can even buy organic frequency doubling crystals on the open market. However, the extension of organic crystal techniques to planar waveguided integrated optics devices is not straightforward and the crystal growth method does not seem to work for all chromophores.

Another technique is to put the chromophores into a polymer matrix, either physically (guest-host solutions) or chemically (side-chain polymers). The polymer is then heated to near the glass transition temperature and the (highly polar) chromophores are aligned by applying a high electric field ($\geq 10^5$ V/cm) across the polymer using either electrodes[17] or a corona discharge.[18] The polymer is subsequently cooled under continued application of the electric field to freeze in the orientation. This technique has the advantages of the flexibility of polymer processing techniques, chemical modification of polymer properties and the ability to make thin film waveguides of good optical quality. Limitations are the fairly low, Boltzmann-limited degree of order one can obtain in the poling field before dielectric breakdown and the tendency of the chromophores to relax after the electric field is removed, limiting the second order susceptibility one can attain in polymers for a given chromophore.

Susceptibilities well above that of the market leader for electro-optics, $LiNbO_3$, have been achieved with polymers which have been deposited in films, structured into waveguides and used to modulate light using the linear electro-optic (Pockels) effect. An example of such a device is shown schematically in Figure 9.[17, 18] The active polymer with refractive index n_K, between cladding layers with n_M, forms a planar waveguide in which the optical electric field $\vec{E}(\omega)$ is confined through total internal reflection. An AC voltage is then applied perpendicular to the substrate and induces, through the Pockels effect, a modulation of the refractive index n in the active polymer (Eq. 4).

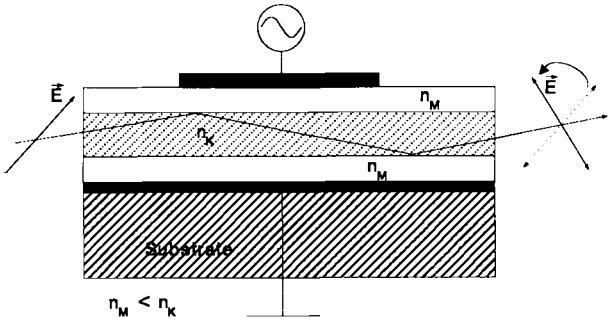

Fig. 9. Slab waveguide electro-optic modulator based on poled polymers

The relationship between the Pockels coefficient Γ and $\chi^{(2)}$ is shown in Equation 5. The εs are the dielectric constants at the optical frequency ω and the much lower modulation frequency Ω. For light polarized diagonally to the substrate, i.e. coupled into TM (electric field perpendicular to the substrate) and TE (electric field parallel to the substrate) modes, the phase of the TM component relative to the TE mode is

$$(n^2)^{-1} = (n_0^2)^{-1} + \Gamma \vec{E} \tag{4}$$

$$\Gamma = \frac{2\chi^{(2)}}{\varepsilon(\omega)\,\varepsilon(\Omega)} \tag{5}$$

modulated. The resulting phase shift causes a rotation of the plane of polarized light; this polarization modulation can be converted to amplitude modulation by the addition of an analyzer after the device.

In order to take advantage of the fast switching times of organics and to design extremely high-speed modulators one must go to more sophisticated architectures which take the finite spatial extent of very short electrical impulses into account (so-called "traveling wave" electrode geometries). The NLO program at the Hoechst Celanese Corporation is

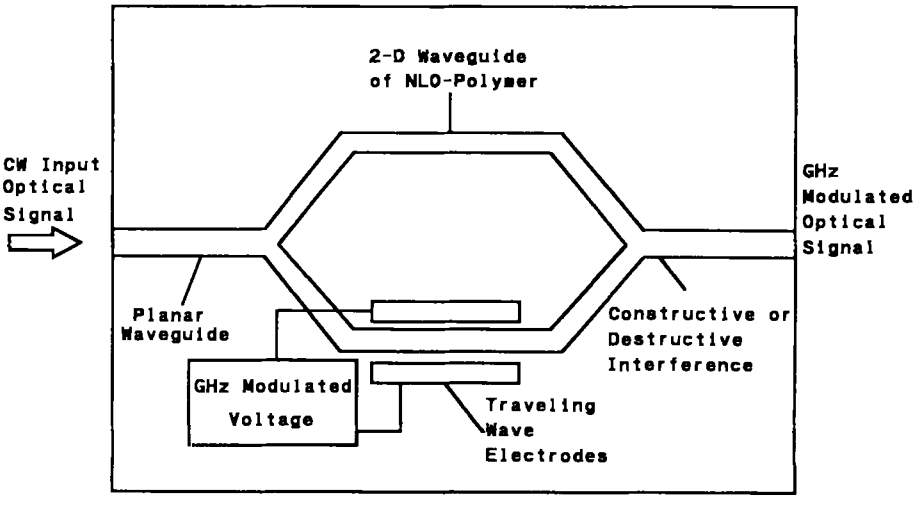

Fig. 10. Schematic representation of a polymeric Mach-Zehnder high frequency electro-optic modulator.

currently developing a multi-GHz traveling wave electro-optic modulator on the basis of a Mach-Zehnder interferometer[19] as shown in Figure 10. The microwave frequency electrical signal runs along a traveling wave electrode across one branch of the interferometer. Depending on the momentary voltage, one brings the two branches into or out of phase with each other, leading to constructive or destructive interference and thus direct intensity modulation of the light. Such devices are currently available based on $LiNbO_3$, but the ultimate attainable bandwidth is substantially less than that for organic materials.

3.2. NLO Active LB-Layers

Our investigations of nonlinear optical effects are focused on Langmuir–Blodgett (LB) films, which, due to their very high and often nearly ideal degree of order, yield the highest $\chi^{(2)}$ values measured to date,[20–22] but which are still at the stage of fundamental investigation. LB films with second order nonlinear optical properties are prepared using amphiphilic dyes, as shown in Figure 11, which contain a hydrophobic "tail", typically an alkyl chain, and a polar hydrophilic "head group", in NLO applications typically a donor-acceptor chromophore. A dilute solution of such species in a volatile solvent such as chloroform or methylene chloride is then spread onto a clean water surface in a film balance or "trough" (Fig. 12, top). After evaporation of the solvent (middle) the monolayer is compressed, leading to a highly oriented monolayer in which the head groups are next to the water surface and the tails are pointed away from it (bottom). This highly oriented monolayer can be transferred to a clean substrate a monolayer at a time, maintaining a high degree of order, by dipping the substrate through the interface into and out of the trough.

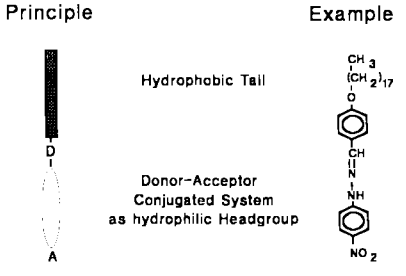

Fig. 11. Design of amphiphilic dyes for LB films with high second order optical nonlinearities.

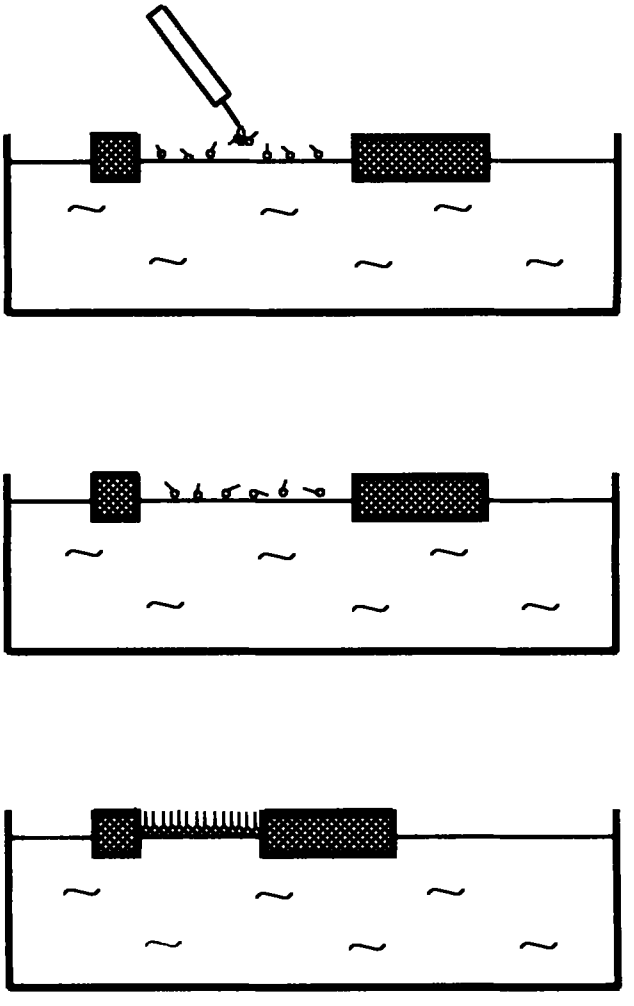

Fig. 12. Creation of oriented monolayers at the air-water interface.

By alternating an NLO active substance with a buffer layer (as shown in Fig. 13) or by alternating layers of molecules whose nonlinearities are in opposite directions with respect to the tails, using specially designed double well troughs, one can built up non-centrosymmetric multilayers with a high degree of order and thus very high susceptibilities. The exact control of film thickness (within the length of one molecule) and the possibility of film architecture on a molecular scale are two of the qualities which make Langmuir–Blodgett films promising for long-range applications in nonlinear integrated optics.

For fundamental studies of structure-property relationships and orientational phenomena, monolayers are practical model systems for study. The high susceptibilities of LB films lead to high signal to noise ratios even for a single

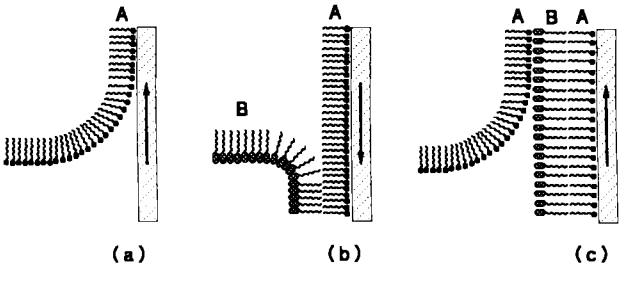

Fig. 13. Deposition of non-centrosymmetric Langmuir-Blodgett multilayers.

ADVANCED MATERIALS

monolayer. The experimental setup for studies of second harmonic generation in LB films is shown in Figure 14. The polarized beam from a pulsed Nd:YAG laser with a wavelength of 1064 nm is passed through the film deposited on a glass substrate, mounted on a rotation stage. Through the second order susceptibility of the film $\chi^{(2)}(-2\omega;\omega,\omega)$ a part of the laser light with circular frequency $\omega = 2\pi c/\lambda_0$ is converted to a harmonic wave at twice the frequency, i.e. with wavelength of 532 nm. The harmonic intensity, normalized by the intensity from a reference sample, is measured for different fundamental and harmonic polarizations as a function of incidence angle θ.

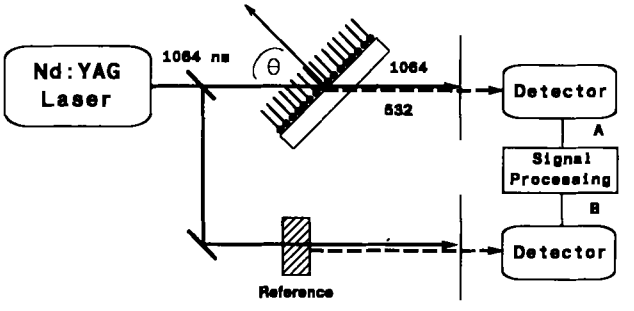

Fig. 14. Experimental apparatus for studying SHG in LB films.

A typical curve for a monolayer of a highly nonlinear hemicyanine dye deposited on both sides of a glass substrate is shown in Figure 15. One sees a superposition of two angular dependences of the second harmonic intensity. The fast fringing pattern is indicative of samples in which the film is deposited on both sides of the substrate and is due to the dispersion in glass between ω and 2 ω, which causes interference between the harmonic waves generated at the front and back surfaces of the substrate. A clean fringing pattern with near zero minima is a good indication of film homogeneity. The shape and height of the slowly varying envelope function depends on the orientation (position of intensity maxima) and the nonlinearity (the height of the curve) of the chromophores in the monolayers. The curve in Figure 15 is consistent with the common assumption that the chromophores are tilted from the substrate normal with a narrow distribution in the tilt angle φ and a statistical distribution in the azimuthal angle. Table 4 shows the nonlinearities and average tilt angles for several amphiphilic dyes which we have investigated.[20] $\chi^{(2)}$ is here a purely scalar quantity with all projection factors removed; the specific tensor components relevant to a particular experiment must be obtained through multiplication by the appropriate projection

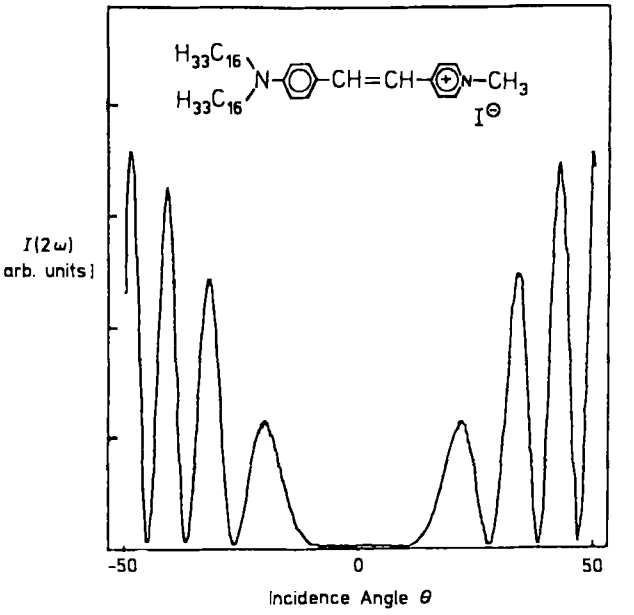

Fig. 15. Dependence of the second harmonic intensity on incidence angle for p-polarized fundamental and harmonic in a hemicyanine monolayer.

Table 4. Nonlinearities and average tilt angles for several amphiphilic dyes.

Structure	$\chi^{(2)}/10^{-6}$ esu	Ave. Tilt Angle/ °
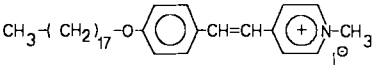	0.51	50
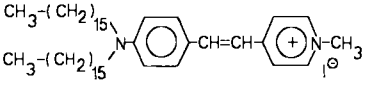	6.25	50
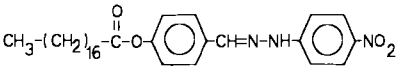	0.56	65
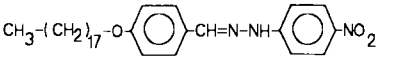	1.80	60
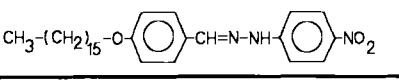	1.70	55

factors. For example, for a TM fundamental and a TM harmonic one would want $\chi^{(2)}_{zzz}$, which is in the simplest approximation given by $\chi^{(2)}_{zzz} \cong \chi^{(2)} \cos^3 \langle \varphi \rangle$.

Second harmonic generation can also be used as a probe of induced changes in orientation in LB films. Figure 16 shows two experimental SHG curves from measurements on the phenylhydrozone ester **1**, pure and diluted with acrylic acid *n*-octadecylamide.[23]

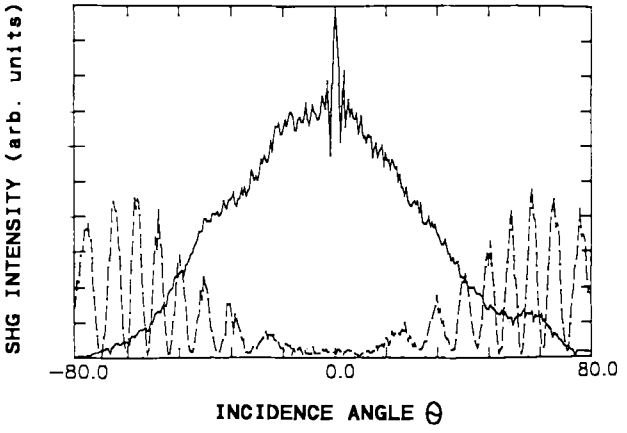

Fig. 16. SHG curves for monolayers of a phenylhydrazone ester, pure (solid line) and diluted with 40% acrylic acid *n*-octadecylamide (dashed line).

The curve for the pure dye is dramatically different from "normal" curves; the lack of fringes indicates poor sample homogeneity and the maximum intensity at normal incidence indicates that the chromophores are lying more or less flat. By diluting the dye with another amphiphilic species one can change the orientation drastically, improving the homogeneity and forcing the chromophores to "stand up".

In order to optimize deposited Langmuir-Blodgett films for nonlinear optics a better understanding of the nonlinear

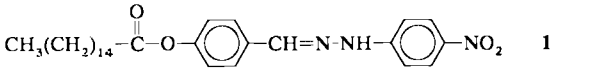

1

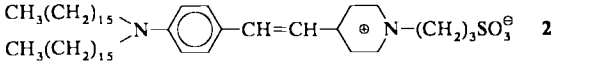

2

optical properties of the monolayer films at the air-water interface is important. Second harmonic generation on reflection from the water surface can be used to monitor in situ the dependence of molecular orientation and nonlinearity on density, surface pressure, and relaxation and aggregation phenomena.[24] The experimental setup is shown schematically in Figure 17. The dependence of the reflected second harmonic intensity on the polarization of the fundamental and the harmonic is monitored as the film is compressed, expanded or held at constant pressure for a period of time. The second harmonic intensity for incidence angle θ is given by Equation 6.

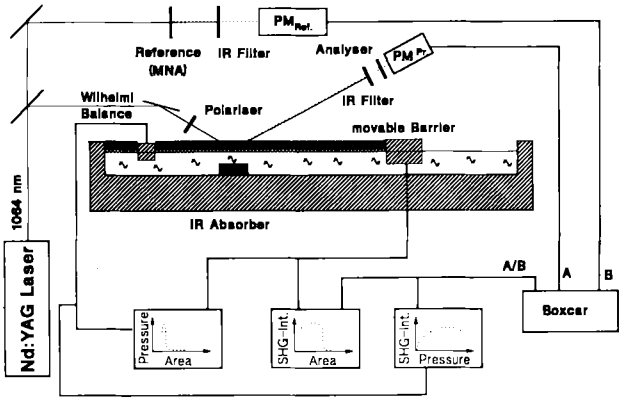

Fig. 17. Experimental apparatus for studies of SHG at the air-water interface.

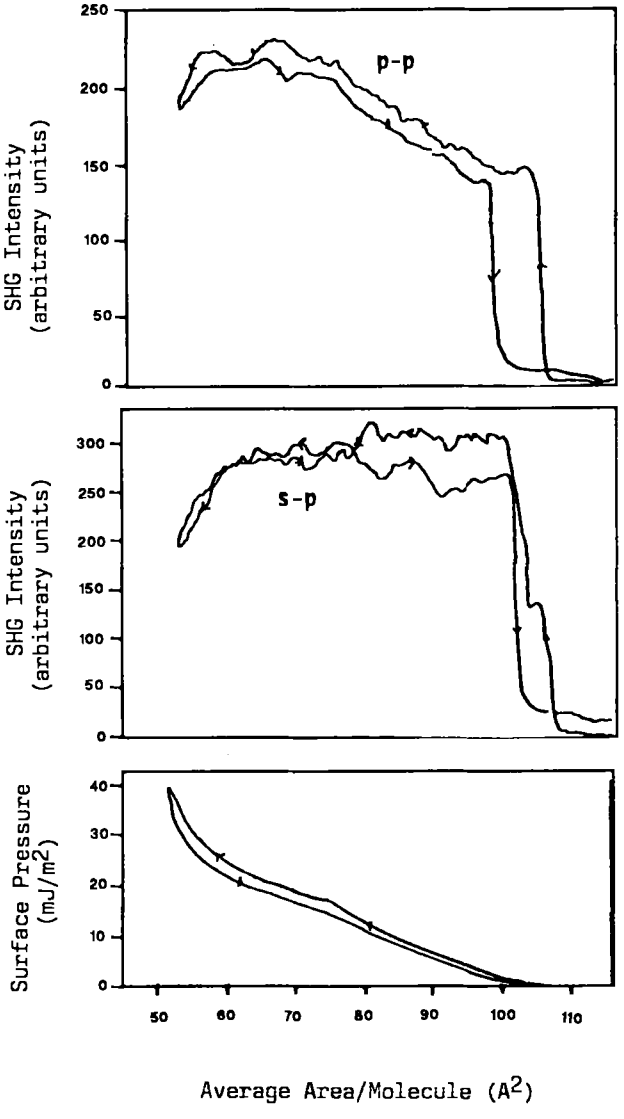

Fig. 18. Dependence of the second harmonic intensity from hemicyanine betaine **2** on water on surface area and the surface pressure-area isotherm. p–p: both fundamental and harmonic are p-polarized; s–p: fundamental is s-, harmonic p-polarized.

$$I(2\omega) = \frac{32\, n^3\, \omega^3 \sec^2\theta}{c^3} |\hat{e}(2\omega) \cdot \chi^{(2)} : \hat{e}(\omega)\hat{e}(\omega)|^2 I(\omega)^2 \qquad (6)$$

where $I(\omega)$ is the intensity of the fundamental, the $\hat{e}$ are the polarization unit vectors for the fundamental and harmonic electric fields, c the speed of light and n the refractive index of the water substrate. The part between the modulus signs accounts for projection factors between fundamental, harmonic and the individual tensor components of $\chi^{(2)}$. Figure 18 shows the second harmonic intensity from the hemicyanine betaine **2** as a function of area per molecule. It is particularly interesting to note that the intensity does not increase significantly over the range of an almost twofold increase in density; in the absence of local field effects or orientational changes one would expect a fourfold increase in intensity over this range of surface areas.

4. Conclusion

A high susceptibility alone is of course not sufficient for applications of Langmuir–Blodgett films in nonlinear optics. Also necessary are high chemical and thermal stability, thick (a few hundred layers) films for planar waveguides with low loss coefficients and methods for forming structures in films without damaging their nonlinear optical properties. Progress has been made in each of these areas individually at Hoechst[25] and elsewhere.[26, 27] Combining all of these properties with high $\chi^{(2)}$ values is now the challenge.

Received August 7, 1989

[1] T. Kaino, M. Fujiki, K. Jinguji, *Rev. Electr. Commun. Lab. 32* (1984) 478.
[2] T. Kaino, *J. Polym. Sci. A 25* (1987) 37.
[3] R. M. Glen, *Chemitronics 1* (1986) 98.
[4] P. Herbrechtsmeier, W. Groh, *Laser und Optoelektronik 20 (5)* (1988) 60.
[5] W. Groh, J. Theis, P. Herbrechtsmeier, J. Coutandin, U. von Alpen, *Elektronikpraxis 10* (1988) 2.
[6] W. Groh, *Makromol. Chem. 189* (1988) 2861.
[7] B. Timm, R. Mecke, *Z. Phys. 98* (1936) 363.
[8] H. Günzler, H. Böck: *IR-Spektroskopie*, Verlag Chemie, Weinheim 1983.
[9] O. H. Wheeler, *Chem. Rev. 59* (1959) 629.
[10] Y. R. Shen: *The Principles of Nonlinear Optics*, Wiley, New York 1984.
[11] D. Williams (Ed.): *Nonlinear Optical Properties of Organic and Polymeric Materials*, Am. Chem. Soc., Washington 1983.
[12] G. Meredith, in J. Messier, F. Kajzar, P. Prasad, D. Ulrich: *Nonlinear Optical Effects in Organic Polymers*, Kluwer, Dordrecht 1989, p. 105, 385.
[13] T. L. Mazely, W. M. Hetherington III, *J. Chem. Phys. 86* (1987) 3640.
[14] P. A. Norman, D. Bloor, J. S. Obhi, S. A. Karavlov, M. B. Hursthouse, P. V. Kolinsky, R. J. Jones, S. R. Hall, *J. Opt. Soc. Amer. B, 4* (1987) 1013.
[15] C. Bosshard, K. Sutter, P. Günter, G. Chapuis, R. J. Twieg, D. Dobrowolski, in R. A. Hann, D. Bloor (Eds.): *Organic Materials for Nonlinear Optics*, R. Soc. Chem., London 1989.
[16] J. Zyss, D. S. Chemla, J. F. Nicoud, *J. Chem. Phys. 74* (1981) 4800.
[17] T. M. Leslie, C. C. Teng, unpublished.
[18] J. E. Sohn, K. D. Singer, M. G. Kuzyk, W. T. Holland, H. E. Katz, C. W. Dirk, M. C. Schilling, R. B. Comozoli, in reference [12]. J. Comizzoli, *J. Electrochem. Soc. 134* (1987) 424.
[19] A. Buckley, J. Stamatoff, in reference [12].
[20] D. Lupo, W. Praß, U. Scheunemann, A. Laschewsky, H. Ringsdorf, I. Ledoux, *J. Opt. Soc. America B5* (1988) 300.
[21] I. R. Girling, P. V. Kolinsky, J. D. Evans, G. H. Cross, I. R. Peterson, *Thin Solid Films 132* (1985) 101.
[22] G. Marowsky, L. F. Chi, D. Möbius, R. Steinhoff, Y. R. Shen, D. Dorsch, B. Rieger, *Chem. Phys. Lett. 147* (1988) 420.
[23] J. Bauer, P. Jeckeln, D. Lupo, W. Praß, U. Scheunemann, R. Keosian, G. Khanarian, in reference [15].
[24] Y. R. Shen, *Annu. Rev. Mater. Sci. 16* (1986) 68.
[25] D. Lupo, W. Praß, U. Scheunemann, *Thin Solid Films*, in press.
[26] R. H. Tredgold, M. C. J. Young, P. Hodge, E. Khoshdel, *Thin Solid Films 151* (1987) 441.
[27] W. L. Barnes, J. R. Sambles, *Surf. Sci. 177* (1986) 399.

Superconductivity at the Temperature of Dry Ice?

J. T. Chen et al. from Wayne State University and the Ford Motor Company recently repeatedly observed zero resistance at temperatures above 200 K in several multi-phase Y-Ba-Cu-O samples. They presented their results at the Third Annual Conference on Superconductivity and Applications held in Buffalo in late September. In the past, *Chen* and others have claimed to have seen evidence of superconductivity above 200 K, but up to now these phenomena turned out to be instable and generally vanished after a few thermal cycles. The key to the stabilization of the effect, *Chen* says, is a low-temperature oxygenation process carried out at temperatures between 50 and 150 °C in an O_2 atmosphere at 0.1 and 13 MPa for four to seven days. Samples were kept in an oxygen atmosphere during all measurements.

Chen et al. prepared samples of various compositions by conventional solid state reaction techniques, but only observed stable zero-resistance phenomena in samples having the nominal composition $Y_5Ba_6Cu_{11}O_y$. X-ray spectra of these samples showed $YBa_2Cu_3O_{7-x}$, Y_2BaCuO_5, and CuO as the predominant phases, but a small number of unidentified peaks were also seen. $YBa_2Cu_3O_{7-x}$ peaks showed preferential orientation with the *c*-axis perpendicular to the surface.

Chen's team determined resistance and current-voltage characteristics by cooling with liquid nitrogen or a mixture of dry ice and acetone. Zero resistance was found in several samples near 250 K. The zero-resistance phenomenon was observed over eleven days and for as many as 29 thermal cycles. Current-voltage characteristics show ohmic behavior at room temperature and an onset of nonlinearity in the range of 260 to 290 K. Magnetization measurements with a SQUID magnetometer did not reveal a complete Meissner effect, but *Chen* et al. observed small diamagnetic deviations and some hysteresis.

Although the findings of the team were well documented and measurements appear to have been done very carefully, there are still some questions that have to be resolved before one can be sure that the observed phenomenon is indeed superconductivity. The fact that zero-resistance was only seen in mixed-phase samples together with the extreme weak diamagnetic signal, could indicate some sort of grain boundary superconductivity, a suggestion *Chen* made in a paper scheduled for the November issue of *Modern Physics Letters B*. The oxygen environment of the samples, even during low temperature measurements, was clearly shown to be crucial, since the zero-resistance state vanished upon evacuating the oxygen atmosphere. It will be interesting to see whether these experiments can be reproduced by *Chen* and, even more importantly, by others.

Herbert Jaeger, Max Planck Institute for Metals Research, Heisenbergstr. 5, D-7000 Stuttgart 80 (FRG)